MULTIPLEXING AND INCREASING THE THROUGHPUT OF "ROLOSENSE ASSAY" UTILIZING COST-EFFECTIVE WIFI IMAGING AND DISPOSABLE MICROFLUIDICS CHIPS FOR SARS-COV-2 DETECTION

Jorge Manrique Castro[1†], *Frank Sommerhage*[2†], *Selma Piranej*[3], *David DeRoo*[2], *Khalid Salaita*[3], *and Swaminathan Rajaraman*[1,2]

[1]University of Central Florida, Orlando FL, USA, [2]Primordia Biosystems, Orlando FL, USA, and [3]Emory University, Atlanta GA, USA

[†] Equally Contributing Authors

ABSTRACT

We present the development of a wireless, standalone device and disposable microfluidics chips that rapidly generate parallel SARS-CoV-2 readouts for selected variants directly using a nasal or saliva sample, based on the Rolosense Assay (RA) [1]. The SARS-CoV-2 test kit consists of a WiFi readout module, a microfluidic chip, and a sample collection/processing sub-system. Here, we focus on the fabrication and characterization of the microfluidic chip to multiplex RA for economic, disposable, and simultaneous detection of up to six different viruses or variants in a single test and data collection using a commercially available, WiFi-capable, and camera-integrated device (Figure 1).

KEYWORDS

Rolosense Assay, High-Throughput (HT), Microfluidics, Multiplexing, Microchannels, Microfabrication.

INTRODUCTION

Microfluidics platforms are being developed and deployed all around us in a variety of ways, starting from single purpose, disposable chips to analyze specific biological samples **[2]**, integrated into a broader system as the initially proposed Micro Total Analysis System (μTAS) for running chemistry on a chip **[3]** or into fully microfluidic-integrated-chip biosensors for organs modeling as demonstrated recently by Ding et al. **[4]**.

In terms of technological development, microfluidics platforms for biomedical applications are moving away from traditional soft lithographic techniques and instead using other novel and cost-effective approaches. For instance, 3D printing based microfluidic chips have been deployed towards bacterial detection **[5]**, and protein purification **[6]**. Additionally, double-sided adhesives based microfluidic fabrication strategies are being developed for microphysiological systems **[7]**. These newer microfabrication strategies are being implemented using novel designs, materials selection and operating at the limits of common microfabrication techniques. One recent review article that illustrates this expansion is from Ingber detailing the approaches to the expansion of microfluidics into more complex platforms as such as human organs-on-chips and personalized medicine **[8]** that allow drug development and disease modeling more efficiently.

Microfluidics are also playing a role in addressing challenges caused by recent global health events. With the advent of the coronavirus disease (COVID-19) and its rapid propagation around the world with multiple, and highly contagious variants, clinical testing of individuals remains not dynamic enough to prevent the spread of rapidly evolving viral targets such as SARS-CoV-2. Several tests both laboratory, and in-home/POC have been deployed to combat the pandemic **[9]**. In contrast to most state-of-the art tests involving microscopy and off-chip assays **[10]**, the Rolosense Assay (RA) does not require complex fluorescence, colorimetric read-outs, nor does the biological sample require exhaustive reverse transcription and DNA amplification as in Polymerase Chain Reaction (PCR) testing.

Single purpose RA requires a nasal swab or saliva sample inserted into a point-of-care (POC) solution detection platform for whole virion detection via DNA motors coated with virus binding ligands. The motors are 5 μm spheres which exhibit motion in the absence of virus and stall in the presence of virus. Microfluidics can increase the throughput of the sample collection chip to run parallel testing. A portable and easy-to-use version of the POC device could be made available over the counter for in-home use. This portable reader with reliable optical readout and wireless functionality can be reused with consumable, disposable microfluidic chips.

In this work, we propose an ***in-home/POC solution*** for ***high-throughput, multiplexed and low-cost RA*** utilizing microfluidics to detect multiple different viruses and/or different variants of viruses (e.g., original COVID-19, Delta, or Omicron variants) in parallel without electrical crosstalk **[11]**, which is eliminated due to optical

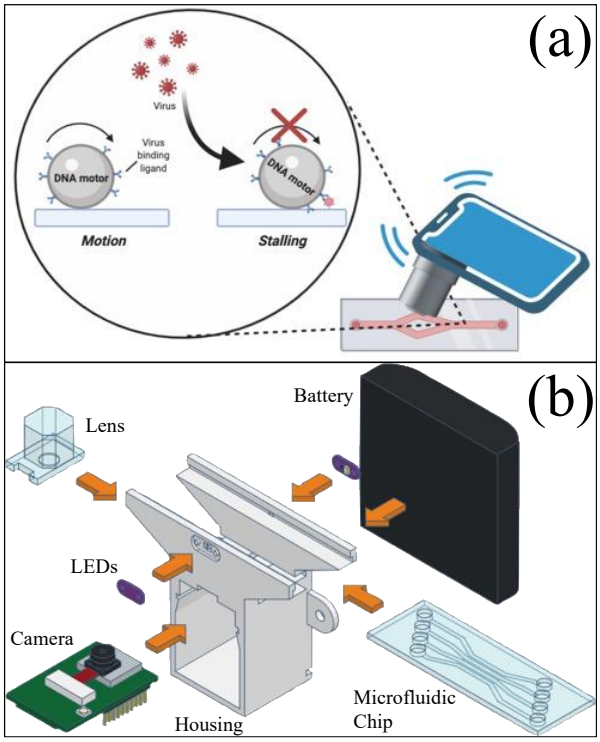

Figure 1. *(a): Traditional Rolosense Assay (RA) set up using a microscope and a cell phone camera. (b): Schematic of the optimized SARS-CoV-2 detection kit, showcasing both cost effective WiFi and disposable microfluidics transmitting RA results wirelessly to the patient phone to visualize optical results in real time, and run post processing virus detection by analyzing the motion of motorized particles, which is the principle of RA.*

978-1-940470-04-7/HH2022/$25©2022TRF
DOI 10.31438/trf.hh2022.4

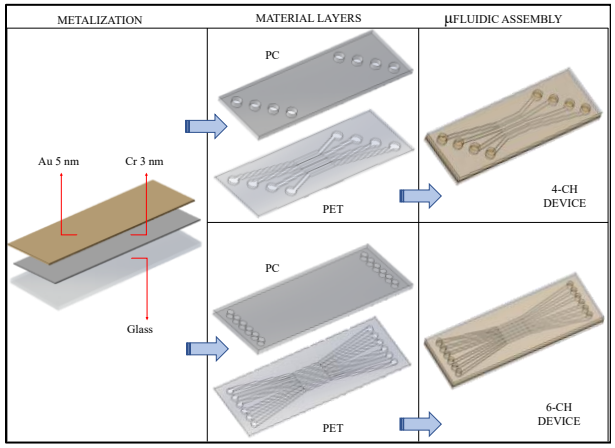

***Figure 2**. Multilayered microfluidic chip microfabrication and assembly. Integration from left to right - metallization: Chromium at 3 nm followed by Gold at 5 nm E-beam deposition on top of the glass substrate. Surface roughness characterization was performed on the top-most layer (Table I). Material Layers: Microfabricated intermediate layers of PET (plotter cut double-side adhesive) and micromilled PC. Surface profile characterization was performed to ports and channels (Table II). Microfluidic Assembly: Integrated chip by bonding all the layers together. Flow and leaking tests were performed successfully.*

detection principle. This assay optimization follows a simple multi-step procedure: sample collection (nasal swab), incubation (chip ports), sample loading/flowing (microchannels) and readout (detection kit + mobile phone).

MATERIALS AND METHODS

Traditional RA requires expensive optical microscope setup to capture images of the motion of 5 µm spheres (DNA motors) with high degree of precision **[12]**, whereas our approach utilizes standard magnification, low-resolution cameras, and sub-pixel motion detection along with WiFi-readiness/data transmission to a central data storage location for tracking the motion of spheres that can additionally be utilized in variant-outbreak detection in a multichannel microfluidic chip.

The WiFi readout module, as depicted in **Figure 1**, is contained in a 3D printed cartridge (Tronxy 820m) and integrates LEDs, basic optics (SuperEyes Lens) and two-core board-level microprocessor electronics (ESP32-CAM module), featuring a two-megapixel camera (OV2640) and an SD card reader. Assay multiplexing is achieved utilizing "Makerspace Microfabrication" technologies **[13]** to develop multilayered, four (4-CH) and six (6-CH) channel microfluidic devices (**Figures 2 & 3**).

Microfluidics devices were designed in CAD software (Solidworks, Dassault Systèmes) in a three-layer system. The top layer, a Polycarbonate (PC) sheet (75x25x1.5 mm) was machined with a specialized tabletop milling tool (Quick Circuit J5, T-Tech). This layer contains four inlet/outlet well ports set (4 mm diameter) or six inlet/outlet well ports set (2 mm diameter) for 4-CH and 6-CH devices respectively. Two different milling bits were implemented to identify the best quality cutting along the device edges and ports. For the 4-CH, a T2 milling bit was used, whereas for the 6-CH a finer T4 bit was used. The middle layer, microchannels were created using precision plotter cutting (Cameo 4, Silhouette) of Polyethylene Terephthalate (PET)-based double-sided adhesive (RTS3851-17, Medco) of size 75x25x0.15 mm, with good optical clarity. The structural composition (construction) of the double side

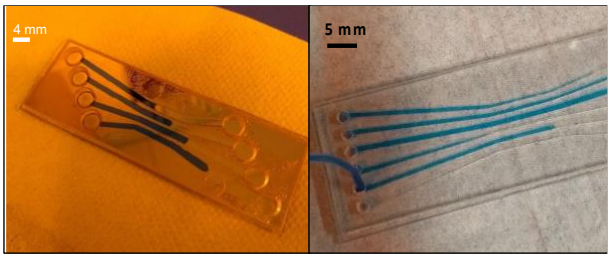

***Figure 3**. Optical images of fully integrated microfluidic chips under flow and leaking tests. Left: 4-CH device Right: 6-CH device. Microfluidic channel widths are between ~1-1.5 mm.*

adhesive is as follows: release film/adhesive/1.0 mil polyester/adhesive/release film. Lastly, the bottom layer comprises a glass substrate that was coated using E-beam evaporator (TC2000, Temescal) with Cr/Au layer (3 nm/5nm thickness) to serve as the microchannel functionalized surface where the RA **[1]** is conducted. All three layers were bonded (**Figures 2 & 3**) and the chip was fully characterized using the portable kit by mimicking RA (**Figures 4 & 5**) with 5 µm microbeads acting as the motors.

Optical characterization of the microfluidic devices (4-CH and 6-CH) was carried out using the WiFi readout module, hosting a browser-based web interface. High-resolution images were saved on an SD card in the ESP-32 CAM module and ported to the web interface. This visualization can be performed by any portable or fixed device with WiFi capability (e.g., smartphones, laptops, desktops, tables, etc.). Particle tracking analysis on captured high-resolution images was performed using motion tracking (Fiji Image J) that identified particles moving in the channels and distances covered. Data was visualized using a custom program (Octave) and scripted python code, comparing particles featuring active RA motors to particles merely moving based on Brownian motion **[14]**.

Physical characterization was performed by measuring surface roughness on channels and ports on 200, 500 and 1000 µm areas, and the dimensions of microchannels width and ports diameter, using laser confocal microscopy (VK-X3000, Keyence) as depicted in **Figures 6 & 7**. This characterization provided information about the accuracy/error of the instruments used in this development process from the design up to the fully assembled devices.

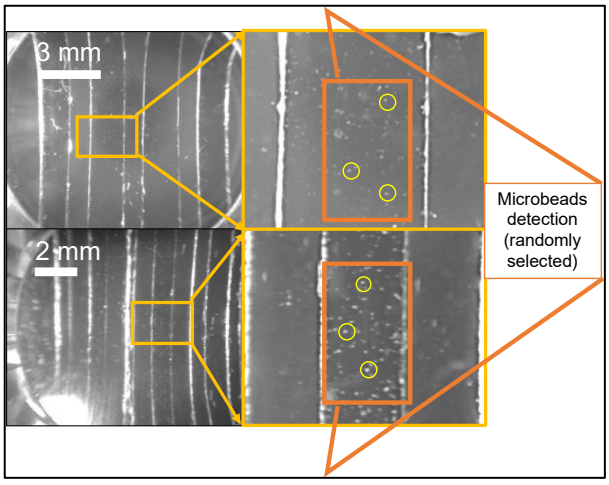

***Figure 4**. Optical micrographs of both 4-CH (top) and 6-CH (bottom) devices with RA being performed in our system. Optical micrographs on the right depict detection of individual 5µm microspheres/microbeads in the images captured by the ESP CAM module.*

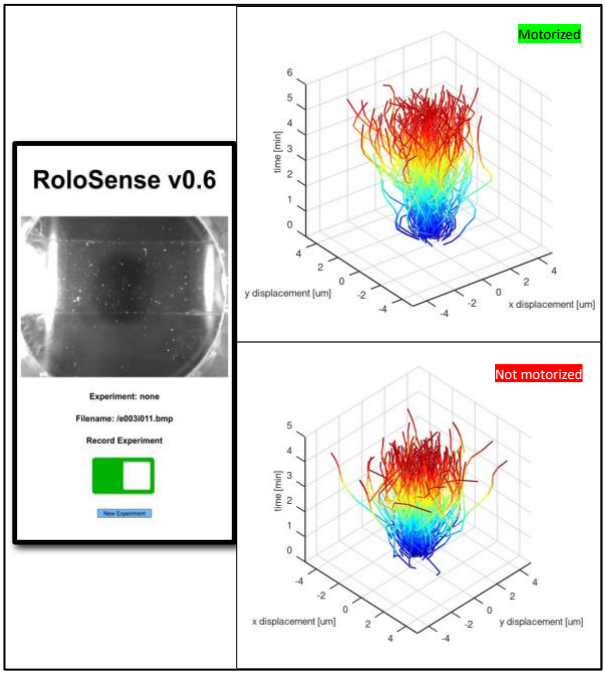

***Figure 5**. Optimized RA results presented as displacement trajectories of the 5 µm spheres in motorized and not motorized conditions in microchannels.*

***Table 1**. Rolosense Assay substrate specification sheet for the 6-channel device after metal deposition and surface characterization.*

ROLOSENSE ASSAY DISPOSABLE MICROFLUIDIC CHIP				
Structure and Materials	Multilayered device: Layer 1: Glass Substrate Layer 2: 3 nm Cr Layer 3: 5 nm Au Layer 4: Microchannels. Double side adhesive PET Layer 5: Ports. PC			
Characterized Material	Cr_3nm/Au_5nm coating			
Version	6-CH			
Instrument used for characterization	3D Surface Profiler			
Instrument used for deposition	E-Beam Evaporator			
Ports. Area under test (µm²)	1000 (n=6)			
Channels. Area under test (µm²)		200 (n=3)	500 (n=6)	1000 (n=3)
Surface Roughness Sa (µm)	0.085	0.034	0.046	0.022

***Table 2.** Microfabrication process specification sheet for PC and PET materials along with Micromilling and Plotter Cutting techniques for the 4 and 6 channels devices.*

ROLOSENSE ASSAY DISPOSABLE MICROFLUIDIC CHIP						
Structure and Materials	Multilayered device: Layer 1: Glass Substrate Layer 2: 3 nm Cr Layer 3: 5 nm Au Layer 4: Microchannels. Double side adhesive PET Layer 5: Ports. PC					
Characterized Material	PC		PET			
Version	4-CH	6-CH	4-CH	6-CH		
Instrument	Micromilling Tool		Cutting Plotter			
Instrument tools	Milling Bit T2	Milling Bit T4	Blade 1			
Settings	Feed rate 20 mm/s Depth of cut 2.2 mm RPM 60k		Force 33 Speed 3 Passes 2 Depth 4			
Port Diameter by design (mm)	4	2	4	2.5	2	1.4
Port Diameter by fabrication (mm)	5.238 (n=4)	2.873 (n=6)	3.834 (n=4)	2.528 (n=6)	1.882 (n=6)	1.409 (n=6)
Channel Width by design (mm)			1.5	1		
Channel Width by fabrication (mm)			1.535 (n=4)	1.118 (n=6)		
Error for Ports (%)	30	43	2.33	1.12	5.9	0.64
Error for Channels (%)			7.73	11.8		

RESULTS AND DISCUSSIONS

Visibility of 5 µm spheres was successfully demonstrated utilizing the wireless kit when implemented on both types of chips. **Figure 4-top** and **bottom** depict beads in the 4-CH chip and 6-CH chip, respectively. Microbeads were identified as bright spots in obtained images. The diameters of microbeads ranged from 4 to 6 pixels, based on background brightness and overall contrast.

Results for sub-pixel motion tracking in an x/y coordinate system representing the microchannel surface is shown in **Figure 5** for motorized and non-motorized particles. Time is represented on the z-axis as well as color (blue = start and red = end of tracking). Data analysis of a subsection of the ***entire frame detected 556 potential 5 µm RA motor spheres and the motion of 227 spheres was successfully tracked for up to 15 minutes.*** Each microparticle's position was normalized and the displacement plotted in superposition. The ***test-spheres traveled between 1 and 4 µm*** under the influence of Brownian motion (**Figures 4 & 5 bottom**).

Surface roughness characterization was performed on the 6-CH chip as a representative of the RA chips used. Design to device errors are observed for the ports which is expected, though the microchannels themselves ***exhibit acceptable (~10%) error*** due to the small displacements between the channel's walls during the mechanical bonding process of the double side adhesive to the metalized substrate.

For the optimal performance of the RA, a flat surface is desired to enhance the chemical-to-mechanical energy exchange of the DNA-motors. An average ***surface roughness of 46.7 nm*** was

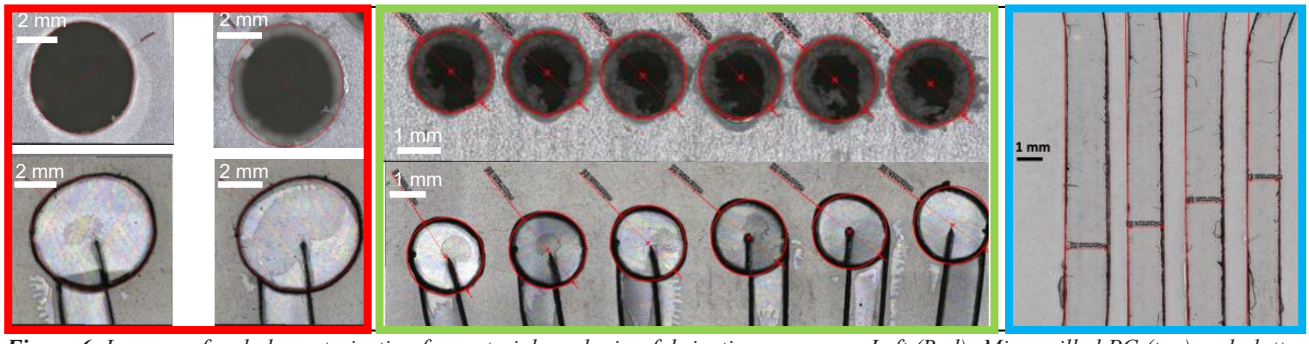

***Figure 6**. Laser confocal characterization for materials and microfabrication processes. Left (Red): Micromilled PC (top) and plotter cut PET (bottom) port diameter measurements for the 4-CH device. Center (Green): Similar measurements for the 6-CH device. Right (Blue): Plotter cut PET channel width measurements for the 4-CH device. All the dimensions and process conditions for 4-CH and 6-CH devices are presented in Table II. Cutting plotter technique revealed to have less error compared to the micromilling approach for the fabrication of ports (~2.5% vs ~36.5%) in both, 4-CH and 6-CH devices. The high error obtained for the micromilling approach, was due to the tapered shape of the milling bit.*

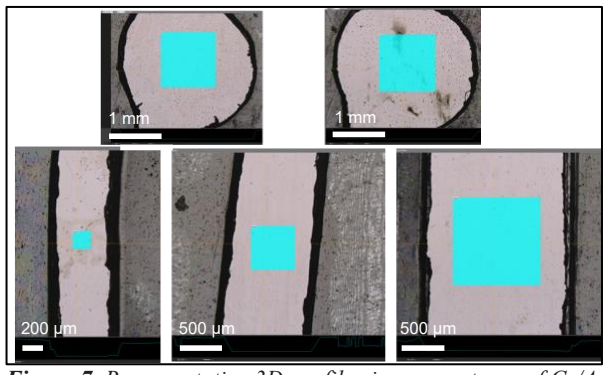

***Figure** 7. Representative 3D profiler image captures of Cr/Au layer surface roughness characterization for the 6-CH device. Ports on top with 1 mm² and channels at bottom with 200 and 500 µm² as evaluation area. Table I (above) presents the roughness value for each case.*

obtained for the 6-CH device, measured at ports and channels over 3 different areas (200, 500 and 1000 µm²) which is excellent for 5µm motor spheres (**Figure 7**). Surface roughness, materials, and microfabrication process specifications for the microfluidics are summarized in **Tables 1 and 2**.

CONCLUSIONS

Combining micromilling along with precise cutting plotter allowed to optimize the microfabrication process for a disposable microfluidic chip. This represents a step forward the multiplexing for detection of several strains of SARS-CoV-2, and paves the way to address incoming challenges with new variants. As the core kit functionality does not depend on the analyzed virus, one-step reagent modification might take place on the surface and motors functionalization to switch from one virus to another.

Cutting plotter provided an acceptable error between design and actual device requirements. This error was mostly due to the manual steps during the bonding process in the multilayered chip. On the other hand, milling tool requires more optimization by using specific purpose bits (e.g., drilling bits) in order to reduce the error on this tool. Its high deviation was caused by the tapered shape of the milling bits, that provided different values for inlet and outlet diameters on the actual ports.

ACKNOWLEDGEMENTS

Authors acknowledge support from the grants NIH U01AA029345-01, Florida High Tech Corridor Match Grants, NSF DMR 1905947, and NSF MSN 2004126.

REFERENCES

[1] K. Yehl *et al.*, "High-speed DNA-based rolling motors powered by RNase H," *Nature Nanotechnology,* vol. 11, no. 2, pp. 184-190, 2016/02/01 2016, doi: 10.1038/nnano.2015.259.

[2] N. Azim, N. Castaneda, A. Diaz, H. Kang, and S. Rajaraman, *MULTI-MODAL MICROELECTRODE ARRAYS FOR THE INVESTIGATION OF PROTEIN ACTIN'S ELECTRO-MECHANOSENSING MECHANISMS TOWARD NEURODEGENERATIVE DISEASE MODELS ON A CHIP*. 2018, pp. 253-256.

[3] A. Manz, N. Graber, and H. M. Widmer, "Miniaturized total chemical analysis systems: A novel concept for chemical sensing," *Sensors and Actuators B: Chemical,* vol. 1, no. 1, pp. 244-248, 1990/01/01/ 1990, doi: https://doi.org/10.1016/0925-4005(90)80209-I.

[4] S. Ding, H. Zhang, and X. Wang, "Microfluidic-Chip-Integrated Biosensors for Lung Disease Models," *Biosensors,* vol. 11, no. 11, 2021, doi: 10.3390/bios11110456.

[5] A. Kundu, T. Ausaf, P. Rajasekaran, and S. Rajaraman, "Multimodal Microfluidic Biosensor With Interdigitated Electrodes (IDE) And Microelectrode Array (MEA) For Bacterial Detection And Identification," in *2019 20th International Conference on Solid-State Sensors, Actuators and Microsystems & Eurosensors XXXIII (TRANSDUCERS & EUROSENSORS XXXIII)*, 23-27 June 2019 2019, pp. 1199-1202, doi: 10.1109/TRANSDUCERS.2019.8808696.

[6] T. Habib, C. Brämer, C. Heuer, J. Ebbecke, S. Beutel, and J. Bahnemann, "3D-Printed microfluidic device for protein purification in batch chromatography," *Lab on a Chip,* 10.1039/D1LC01127H vol. 22, no. 5, pp. 986-993, 2022, doi: 10.1039/D1LC01127H.

[7] S. Hosic *et al.*, "Rapid Prototyping of Multilayer Microphysiological Systems," *ACS Biomaterials Science & Engineering,* vol. 7, no. 7, pp. 2949-2963, 2021/07/12 2021, doi: 10.1021/acsbiomaterials.0c00190.

[8] D. E. Ingber, "Human organs-on-chips for disease modelling, drug development and personalized medicine," *Nature Reviews Genetics,* 2022/03/25 2022, doi: 10.1038/s41576-022-00466-9.

[9] H. Safiabadi Tali Seyed *et al.*, "Tools and Techniques for Severe Acute Respiratory Syndrome Coronavirus 2 (SARS-CoV-2)/COVID-19 Detection," *Clinical Microbiology Reviews,* vol. 34, no. 3, pp. e00228-20, doi: 10.1128/CMR.00228-20.

[10] S. Fuchs, S. Johansson, A. Ø. Tjell, G. Werr, T. Mayr, and M. Tenje, "In-Line Analysis of Organ-on-Chip Systems with Sensors: Integration, Fabrication, Challenges, and Potential," *ACS Biomaterials Science & Engineering,* vol. 7, no. 7, pp. 2926-2948, 2021/07/12 2021, doi: 10.1021/acsbiomaterials.0c01110.

[11] J. Fu, L. Wu, Y. Qiao, J. Tu, and Z. Lu, "Microfluidic Systems Applied in Solid-State Nanopore Sensors," *Micromachines,* vol. 11, no. 3, 2020, doi: 10.3390/mi11030332.

[12] A. Bazrafshan *et al.*, "DNA Gold Nanoparticle Motors Demonstrate Processive Motion with Bursts of Speed Up to 50 nm Per Second," *ACS Nano,* vol. 15, no. 5, pp. 8427-8438, 2021/05/25 2021, doi: 10.1021/acsnano.0c10658.

[13] A. Kundu, T. Ausaf, and S. Rajaraman, "3D Printing, Ink Casting and Micromachined Lamination (3D PICLµM): A Makerspace Approach to the Fabrication of Biological Microdevices," (in eng), *Micromachines,* vol. 9, no. 2, p. 85, 2018, doi: 10.3390/mi9020085.

[14] S. Piranej, A. Bazrafshan, and K. Salaita, "Chemical-to-mechanical molecular computation using DNA-based motors with onboard logic," *Nature Nanotechnology,* 2022/03/28 2022, doi: 10.1038/s41565-022-01080-w.

CONTACT

*Swaminathan Rajaraman, tel: +1-407-823-4339; swaminathan.rajaraman@ucf.edu